C. R. Chimie 17 (2014) 869–880

Contents lists available at ScienceDirect

Comptes Rendus Chimie

www.sciencedirect.com

Full paper/Mémoire

Kinetic and equilibrium studies of lead(II) adsorption from aqueous media by KIT-6 mesoporous silica functionalized with –COOH☆

Études cinétiques et d'équilibre d'adsorption du plomb(II) en milieux aqueux sur une silice mésoporeuse KIT-6 fonctionnalisée par COOH

Nabila Bensacia [a,b], Ioana Fechete [a,*], Saâd Moulay [b], Oana Hulea [a], Anne Boos [c], François Garin [a]

[a] *Institut de chimie et procédés pour l'énergie, l'environnement et la santé (ICPEES), UMR 7515 CNRS, Université de Strasbourg, 25, rue Becquerel, 67087 Strasbourg cedex 2, France*
[b] *Laboratoire de chimie physique moléculaire et macromoléculaire, département de chimie industrielle, faculté des sciences de l'ingénieur, Université Saâd-Dahlab de Blida, BP 270, route de Soumâa, 09000 Blida, Algeria*
[c] *Institut pluridisciplinaire Hubert-Curien (IPHC), UMR 7178 CNRS, Université de Strasbourg, 25, rue Becquerel, 67087 Strasbourg cedex 2, France*

ARTICLE INFO

Article history:
Received 6 February 2014
Accepted after revision 10 March 2014
Available online 18 April 2014

Keywords:
Kinetic studies
Adsorption
Lead(II)
COOH/KIT-6

ABSTRACT

An organic–inorganic hybrid mesoporous silica was synthesized via post-grafting of KIT-6 with 4-(triethoxysilyl)butyronitrile. All samples were characterized using their N_2 adsorption–desorption isotherms, XRD, FT–IR, TEM, SEM, and PT. The adsorption potential of this material for removing Pb(II) from aqueous solutions was investigated via the batch technique, and the effects of pH and contact time were studied. Experimental data showed that the maximum Pb(II) adsorption, 76%, occurred in the pH range around 6. The adsorption equilibrium was reached within 40 min for 10 wt.%COOH/KIT-6. The adsorption data were fitted using the Langmuir and Freundlich isotherms, and the obtained modeling equilibrium adsorption data suggested that the 10 wt.%COOH/KIT-6 sample contained homogeneous adsorption sites that fit the Langmuir adsorption model well. The pseudo-second-order model described well the 10 wt.%COOH/KIT-6 adsorption process. The desorption and regeneration experiments indicated that ≈95% of the metal desorbed and the adsorbent could be regenerated via an acid treatment without altering its properties.

Mots clés :
Étude cinétique
Adsorption
Plomb(II)
COOH/KIT-6

RÉSUMÉ

Une silice mésoporeuse hybride organique–inorganique a été synthétisée par greffage du KIT-6 avec le 4-(triéthoxysilyl)butyronitrile. Les échantillons ont été caractérisés par BET, XRD, FT–IR, MET, MEB et TP. Le potentiel d'adsorption de la silice mésoporeuse pour éliminer Pb(II) à partir de solutions aqueuses a été étudié par la technique de traitement par lots. Les effets du pH et du temps de contact ont aussi été analysés. Les données expérimentales montrent que l'adsorption maximale de Pb(II) est de 76 % et a lieu dans une plage de pH entre 5 et 6. L'équilibre d'adsorption a été atteint en 40 minutes pour le 10 wt.%COOH/KIT-6. Les

☆ Thematic issue dedicated to François Garin.

* Corresponding author. Institut de chimie et procédés pour l'énergie, l'environnement et la santé (ICPEES), UMR 7515 CNRS, Université de Strasbourg, 25, rue Becquerel, 67087 Strasbourg cedex 2, France.
E-mail addresses: ifechete@unistra.fr, ifechete@voila.fr (I. Fechete).

http://dx.doi.org/10.1016/j.crci.2014.03.007
1631-0748/

données d'adsorption ont été analysées à l'aide des isothermes de Langmuir et de Freundlich. Les données obtenues par la modélisation ont suggéré que l'échantillon 10 wt.%COOH/KIT-6 contenait des sites d'adsorption homogènes qui correspondent mieux au modèle d'adsorption de Langmuir. Le modèle de pseudo-second-ordre décrit mieux le processus d'adsorption du 10 wt.%COOH/KIT-6. Les expériences de désorption et de régénération ont indiqué qu'environ 95 % des métaux sont désorbés et l'adsorbant 10 wt.%COOH/KIT-6 peut être régénéré par un traitement à l'acide, sans modifier ses propriétés.

1. Introduction

Environmental pollution is a planetary problem that still threatens human health and ecosystems worldwide [1–4]. Current rigorous regulations have made global environmental pollution (air, soil, water) a major worldwide problem [5–8]. Over the years, scientists have researched a solution to decrease or eliminate the impact of environmental pollution [9–14]. Potable water is essential for human existence and the ecosystem, and has been widely studied [15–24]. Heavy metals are a major pollutant of wastewaters; they primarily originate from anthropogenic activities and have become a major environmental issue due to their toxicity. Heavy metals are not biodegradable and tend to accumulate in living organisms [25–28]. Many heavy metal ions are known to be toxic or carcinogenic. Among the metals that are hazardous to the environment, lead is considered very toxic. High levels of lead can be traced to industrial discharges from a variety of sources, such as batteries, cables, plastics, paints, and the glass industry. Lead contamination also occurs from vehicular traffic effluents. Although inorganic lead is a general metabolic poison and enzyme inhibitor, its organic forms are even more poisonous [29]. Acute lead poisoning has been known to affect the gastrointestinal tract, nervous system or both. Lead can damage the central nervous system. It can also damage the kidney, liver, reproductive system, basic cellular processes and brain function. The toxic symptoms include anemia, insomnia, headache, dizziness, irritability, muscular weakness, hallucinations and renal failure [30]. Therefore, industrial effluents with high lead content must be treated before being released into the environment. Eliminating such metal ions from water and wastewater has become a challenge for researchers. Various techniques have been used to remove metal ions from aqueous solutions, such as ion exchange, reverse osmosis, membrane filtration, evaporative recovery, phytoextraction, precipitation, conventional coagulation, precipitation, sedimentation, electrodialysis, electrochemical treatments and adsorption [31–34]. However, adsorption is considered more appropriate for removing heavy metals. The adsorption process offers a flexible design and operation and generally yields high-quality treated effluents. In addition, because adsorption is sometimes reversible, the adsorbents can be regenerated via suitable desorption processes. Various adsorbents have been used to remove heavy metals from aqueous solutions [35–42]. The demand to develop novel, high-efficiency adsorbents to remove heavy metal ions from aqueous media is growing. The discovery of siliceous mesoporous materials started a new era in the chemistry of porous solids and renewed the interest in designing heavy metal adsorbents. These mesoporous materials exhibit unique properties, such as uniform pore diameter, large specific surface area, large pore volume, highly ordered pore arrangement, good mechanical and thermal stabilities and free surface silanol groups [43], for versatile applications.

Currently, different mesoporous materials are tested for various possible applications: heterogeneous catalysis [44–48], electrochemical battery components/electrode materials [49,50], heavy metal adsorption [51–54], analytical chemistry [55], and the immobilization of enzymes and of other biologically active molecules [56,57].

Furthermore, one of mesoporous silica's most important properties is its potential to modify its chemical surface to incorporate organic functional groups. Adding organic groups by grafting organosiloxane precursors to the pore surface yields functional mesoporous hybrid materials with improved thermal, mechanical, and chemical stabilities.

Mesoporous hybrid materials also show promise as adsorbents for removing heavy metals from aqueous solutions. These hybrid compounds are classified into two categories: (i) those held together via weak forces, such as van der Waals forces, hydrogen bonding, electrostatic (London) and p–p interactions and (ii) those with covalent bonds between the organic and inorganic parts and functional groups inserted onto the porous silica framework. Functional chemical groups on the porous surface are most often amino, mercapto, or carboxylic groups obtained via either co-condensation or post-grafting. Several studies reported the use of mercapto and amino groups; however, only a few articles have studied carboxylic groups [58–61].

According to a bibliographic survey, there has been no study on the Pb(II) adsorption to COOH/KIT-6. Therefore, this work investigated the adsorption of Pb(II) by COOH/KIT-6 from an aqueous solution. During the co-condensation process, the functional groups can destabilize the solid mesoporous framework [62] and, in this case, our work grafted the carboxylic groups by covalently linking free and geminal silanol groups on the surface of the KIT-6 support. Adsorption is a very complex process, and its characteristics were evaluated as a function of the process variables such as pH, contact time, and temperature. Equilibrium data were examined using the Langmuir and Freundlich isotherm models.

2. Experimental

2.1. Materials

All chemicals used in this study were of analytical grade. Polyethylene oxide–polypropylene oxide–polyethylene

oxide type block copolymer, Pluronic P123, (M_n = 5800), tetraethyl orthosilicate (TEOS, 98%), and hydrochloric acid (HCl, 37%) were purchased from Sigma-Aldrich. The solvents were toluene (Tol), ethanol (EtOH), butanol (BuOH) and sulfuric acid (H_2SO_4), and were purchased from Sigma-Aldrich. All chemicals and solvents were used as received. Milli-Q deionized water was used for all experiments.

The grafting agent was 4-(triethoxysilyl)butyronitrile ($(EtO)_3$Si-BuCN, 97%, Sigma-Aldrich).

2.2. Synthesis of mesoporous KIT-6

The KIT-6 sample was synthesized via the cooperative assembly of surfactants or block copolymer micelles (P123) with an associated silica species in aqueous media [63,64]. P123 was added to distilled water and HCl under stirring. After the surfactant was dissolved, BuOH was added at 35 °C followed by TEOS. The final molar composition of the gel was as follows: 1.00 TEOS:0.017 P123:1.83 HCl:195 H_2O:1.31 BuOH. The gel was stirred for 24 h at 35 °C before being sealed, transferred into an autoclave, and heated at 100 °C for 24 h. The resultant white precipitate was filtered out and dried at 60 °C for 24 h.

2.2.1. Surfactant removal

The occluded surfactant was removed via three steps: (1) reflux in 95% EtOH for 24 h before filtering, washing several times with H_2O and EtOH, and drying at 50 °C; (2) calcination at 550 °C under N_2 for 1 h and air for 4 h to combust the remaining surfactant; (3) immersion in EtOH for 6 h at 40 °C.

2.3. COOH/KIT-6: preparation via post-synthesis grafting

KIT-6 with covalently attached carboxyl groups was formed through several liquid-phase reactions. Excess water was removed from the pores of 2 g of mesoporous KIT-6 by drying at 110 °C for 36 h. The sample was dispersed in 200 mL of toluene under ultrasonic stirring, and the necessary quantity of $(EtO)_3$Si-BuCN was added at room temperature under argon under stirring for 24 h. The grafting reaction was performed under argon while refluxing in toluene for 24 h. The resultant precipitate was then washed in a Soxhlet apparatus with toluene (2 h) and then ethanol for 24 h. This wash was followed by heat treatment at 60 °C for 12 h under vacuum ($< 10^{-2}$ bar).

2.3.1. Oxidation CN

The CN/KIT-6 was acidified with H_2SO_4 for 24 h at 80 °C to produce the COOH/KIT-6.

2.4. Characterization methods

All materials were characterized using various physicochemical techniques to obtain the necessary structural, compositional, and porosity information and enable an appropriate discussion of the analytical results.

2.4.1. Potentiometric titration

The experiments of potentiometric titration (PT) were performed at room temperature and each titration was repeated four times. Sample solutions containing 100 mg of COOH/KIT-6 and 120 mL of 1 M NaCl were potentiometrically titrated with 0.05 M NaOH. The potential data were acquired after a 20-min equilibration after adding the titrant.

2.4.2. Scanning electron microscopy

The scanning electron microscopy (SEM) images were obtained using a JEOL electron microscope 6700 scanning electron microscope operated at 200 kV on a thin film dispersed on a holly carbon grid.

2.4.3. Transmission electron microscopy

A transmission electron microscopy (TEM) study of non- and carboxyl-functionalized KIT-6 samples was performed using a TopCon 2100 FCs microscope operating at 200 kV with very low illumination to avoid destroying the material with the electron beam. The samples were crushed and dispersed ultrasonically in acetone at room temperature and spread onto a perforated carbon–copper microgrid.

2.4.4. N_2 adsorption–desorption isotherms

The textural properties of the mesoporous matrices were determined from the nitrogen adsorption isotherms recorded at −196 °C using a Micromeritics TriStar apparatus. Before the adsorption experiments, each sample was dried at 100 °C for 12 h under vacuum to ensure a clean, dry surface free of any loosely adsorbed species. The specific areas of the samples were calculated via the standard BET procedure using the nitrogen adsorption data collected at a relative equilibrium pressure interval. The total pore volume was estimated from the amount of nitrogen adsorbed at a relative pressure of 0.99. The pore size distributions were calculated from the adsorption and desorption branches of the corresponding nitrogen isotherm via the BJH method.

2.4.5. X-ray diffraction

The structural order of the materials was evaluated via powder X-ray diffraction (XRD). The XRD patterns were recorded using a Bruker D8 powder diffraction system with a Cu Kα radiation source of 1.54 Å wavelength and equipped with a graphite monochromator. The diffraction patterns were collected under ambient conditions across the low-angle 0.5–4° range.

2.4.6. Fourier transform infrared

The Fourier transform–IR (FT–IR) spectra of the mesoporous carboxyl-functionalized adsorbents COOH/KIT-6 were recorded using a Digilab Excalibur 3000 instrument with 128 scans in the mid-IR (4000–400 cm^{-1}) region via the KBr pellet technique.

2.5. Heavy metal adsorption experiments

The adsorption of Pb(II) by the functionalized and non-functionalized mesoporous KIT-6 was studied using batch experiments. We investigated the effects of contact time, solution pH and temperature. These batch sorption experiments were performed in a shaker incubator at

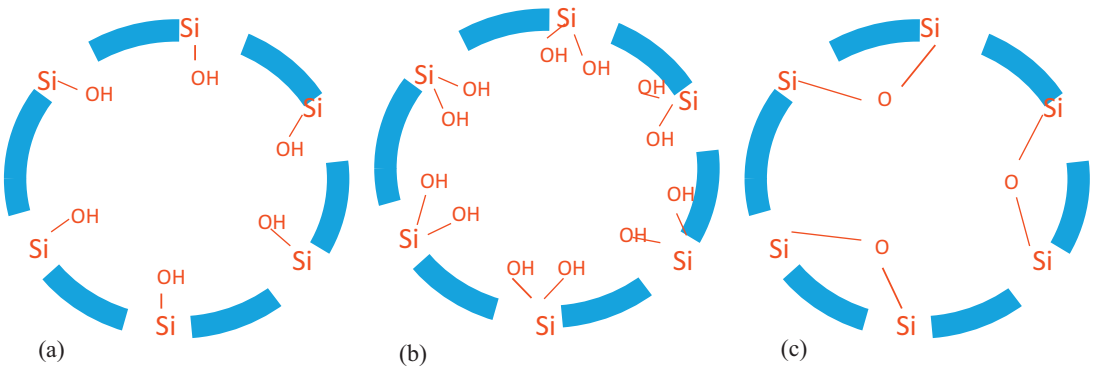

Scheme 1. Types of silanols on the surface of mesoporous silica: free (a), geminal (b), and etherial (c).

150 rpm for 2 h using capped 50 mL plastic centrifuge tubes containing 0.01 g/L Pb(II) solutions and 0.02 g of the adsorbents. The solution pH was adjusted using 0.1 mol/L HCl or NaOH. All of these experiments were performed four times, and the average results are presented.

The percent of metal ion adsorption (A) was calculated using Eq. (1):

$$A(\%) = \frac{C_0 - C_e}{C_0} \times 100 \quad (1)$$

The Pb adsorption capacity was calculated using Eq. (2):

$$q_e = \frac{V(C_0 - C_e)}{w} \quad (2)$$

where C_0 and C_e represent the initial and equilibrium metal ion concentrations ($g{\cdot}L^{-1}$), respectively, V is the metal ion solution volume (L), and w is the amount of adsorbent (g).

3. Results and discussion

3.1. Preparation and characterization of KIT-6 and COOH/KIT-6

Knowing the surface chemistry of a mesoporous solid in aqueous media is very important. The hydrophilic character of the silica surface allows water to rapidly penetrate to its internal pore spaces. The porous solid contains silanol groups on its internal and external surfaces that can anchor organic functional groups to provide the sorbent chemical selectivity for specific molecules and ions. Three silanol groups exist on the ordered nanoporous silica surface. They are free, geminal, and hydrogen-bonded hydroxyl (etherial) groups (Scheme 1), whereas only free and geminal silanol groups react with the functional groups. The types and number of these groups depend on the way the template was removed and the post-treatment process [65]. To preserve the free and geminal silanol groups, we liberated the sample pores via an extraction/calcination followed by an alcohol treatment before the grafting procedure. Furthermore, CN functional groups were covalently incorporated into the nanoporous silica via a post-grafting strategy (Scheme 2). These CN groups were hydrolyzed using H_2SO_4 to generate COOH (Scheme 2). The success of the grafting procedure was confirmed using several physicochemical techniques.

3.1.1. XRD

The XRD pattern of samples exhibited a distinguishable peak at approximately $2\theta = 1.05^\circ$ with a broad peak at $2\theta = 1.27^\circ$, which indicates that the sample possesses a highly ordered mesostructure (Fig. 1). The first peak in the low-angle region was indexed to the (211) reflection in the bicontinuous cubic *Ia*3*d* space group [63,66] and the second peak to the (220) reflection. The interplanar spacing, *d*, was evaluated from the first peak, corresponding to the (211) reflection and the unit cell parameter, a_0, was calculated as $a_0 = d_{211}\sqrt{6}$ (Table 1). These results indicate that the long-range structural order is maintained for the COOH/KIT-6 materials after the grafting and subsequent calcination steps.

3.1.2. BET

The BET specific surface areas and pore distributions for the KIT-6 and COOH/KIT-6 adsorbents are presented in Table 1. The corresponding isotherms are shown in Fig. 2. All of the functionalized samples exhibit N_2 adsorption/desorption curves similar to that of the parent mesoporous silica *Ia*3*d* KIT-6 sample. These results confirmed the mesoporous nature of all of the samples and indicated that

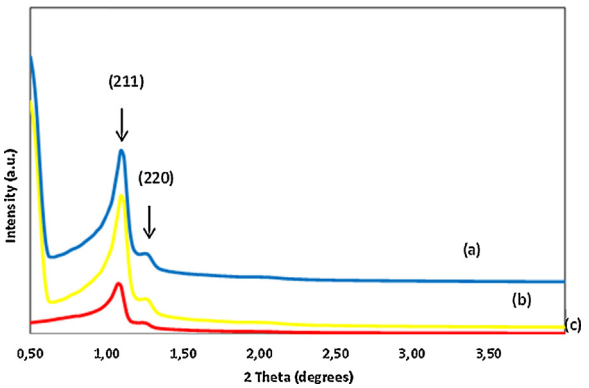

Fig. 1. (Color online). Low-angle XRD patterns of KIT-6 (a), 1 wt.%COOH/KIT-6 (b) and 10 wt.%COOH/KIT-6 (c).

Table 1
Textural and structural properties of the mesoporous solids.

Sample	S_{BET} ($m^2.g^{-1}$)	D_p (nm)	V_p ($cm^3.g^{-1}$)	a_0 (nm)
KIT-6	817	8.6	1.52	19.7
1wt.%COOH/KIT-6	790	8.2	1.40	19.7
10wt.%COOH/KIT-6	525	6.9	0.80	20.6
10wt.%COOH/KIT-6 (6 h)	525	6.9	0.80	20.6
10wt.%COOH/KIT-6 (24 h)	525	6.9	0.80	20.6
10wt.%COOH/KIT-6 (240 h)	525	6.9	0.81	20.6

the mesoporous structure is retained after the grafting and thermal treatment steps. The isotherms are type IV with an H1 hysteresis loop, which is typical for highly organized mesoporous materials [67]. However, it must be noted that introducing carboxylic groups decreased the surface area and pore volume (Table 1).

3.1.3. TEM

TEM studies were conducted for all samples (Fig. 3). The TEM images indicate that the samples had highly ordered cubic mesostructures with well-ordered cubic pores arrays. These results suggest that the ordered KIT-6 mesostructure was not destroyed for any sample, but remained unchanged after incorporating the carboxylic groups via post-grafting. These mesoporous solids exhibited a highly ordered porous arrangement that certainly contributes to Pb sorption.

3.1.4. SEM

Fig. 4 shows the SEM images of the non-functionalized mesoporous silica KIT-6 support (Fig. 4a) and both COOH/KIT-6 solids (Fig. 4b,c). These images showed the typical rock-like morphologies with aggregated grains between 50 and 400 nm usually observed for KIT-6 [64,66]. The samples were irregularly sized and shaped. No significant change in the adsorbent surfaces was observed before and after COOH grafting.

3.1.5. IR spectrum of CN/KIT-6

The IR spectrum of CN/KIT-6 is shown in Fig. 5a. The peak observed at 2260 cm^{-1} was assigned to the vibration of CN bonds. The IR spectrum of 10 wt.%COOH/KIT-6 is shown in Fig. 5b. The peaks attributed to the carboxyl groups were obvious at 1721 cm^{-1} (the stretching of the C=O bond), 1415 cm^{-1} (the bending of the O–H bond), 1282 cm^{-1} (the stretching of the C–O bond), and 897 cm^{-1} (the bending of the O–H bond).

3.1.6. Water stability of 10 wt.%COOH/KIT-6 materials

Mesoporous silica hybrids are some of the most studied sorption materials for heavy metals due to their interesting pore architecture and surface chemistry. It does not swell in water like many organic materials and has both good mechanical strength and excellent thermal stability. In this context, water stability is an important propriety of porous materials. A 10%wt.COOH/KIT-6 sample was tested in

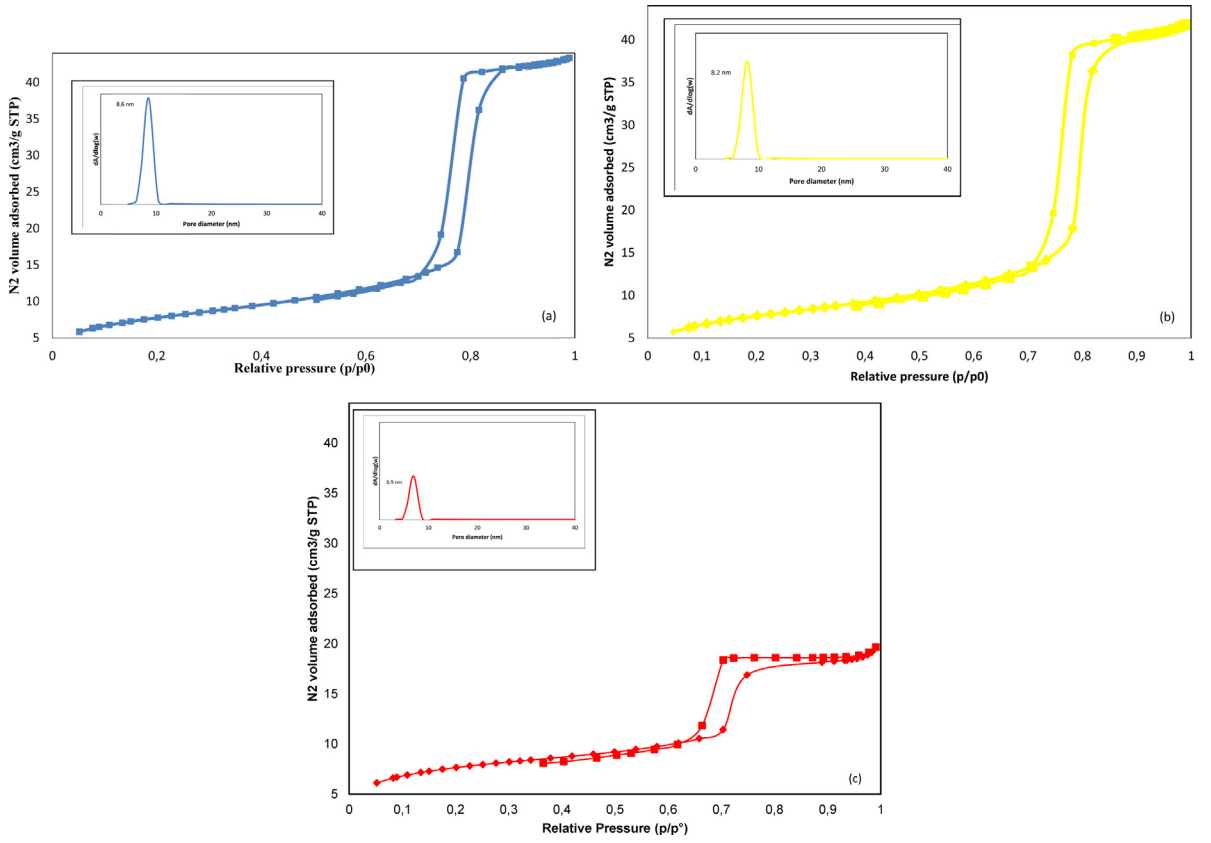

Fig. 2. (Color online). N_2 adsorption/desorption isotherms of KIT-6 (a), 1 wt.%COOH/KIT-6 (b) and 10 wt.%COOH/KIT-6 (c).

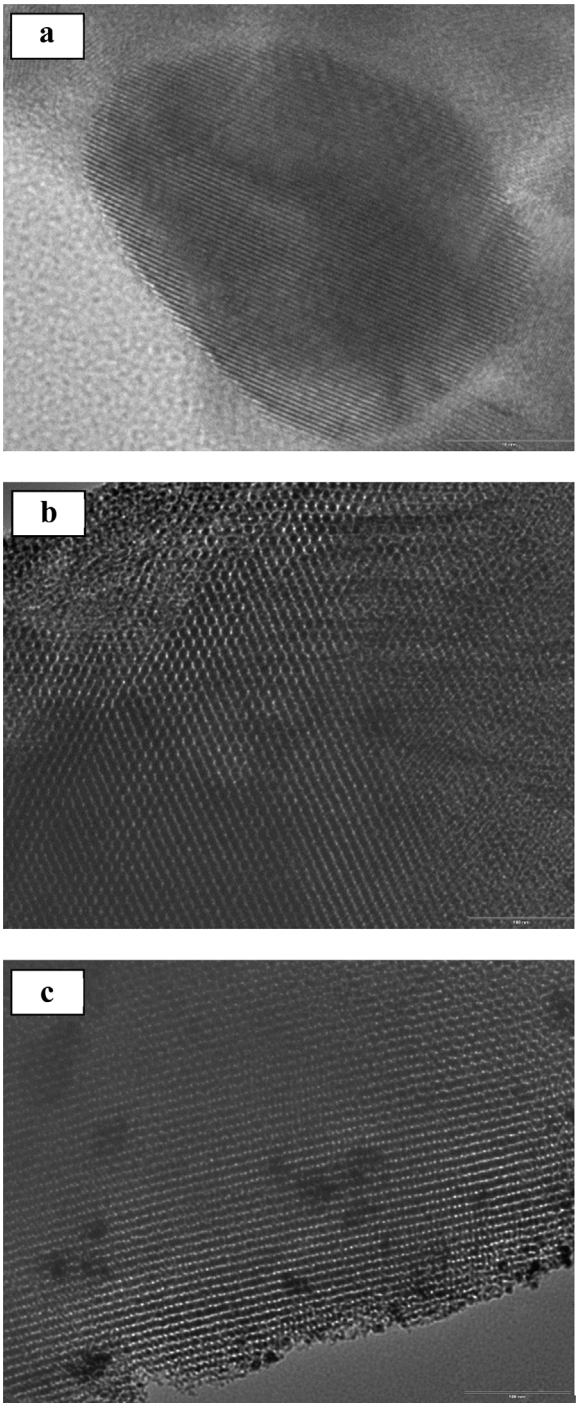

Fig. 3. TEM micrographs of KIT-6 (a), 1 wt.%COOH/KIT-6 (b) and 10 wt.%COOH/KIT-6 (c).

water for 6 h, 24 h and 240 h and monitored via low-angle N_2 sorption (Fig. 6), XRD (Fig. 7) and TEM (Fig. 8). No changes in the XRD, BET surface area and TEM were observed (Table 1). Notably, no sample degradation occurred in these conditions and the 10%wt.COOH/KIT-6 sample presents excellent stability.

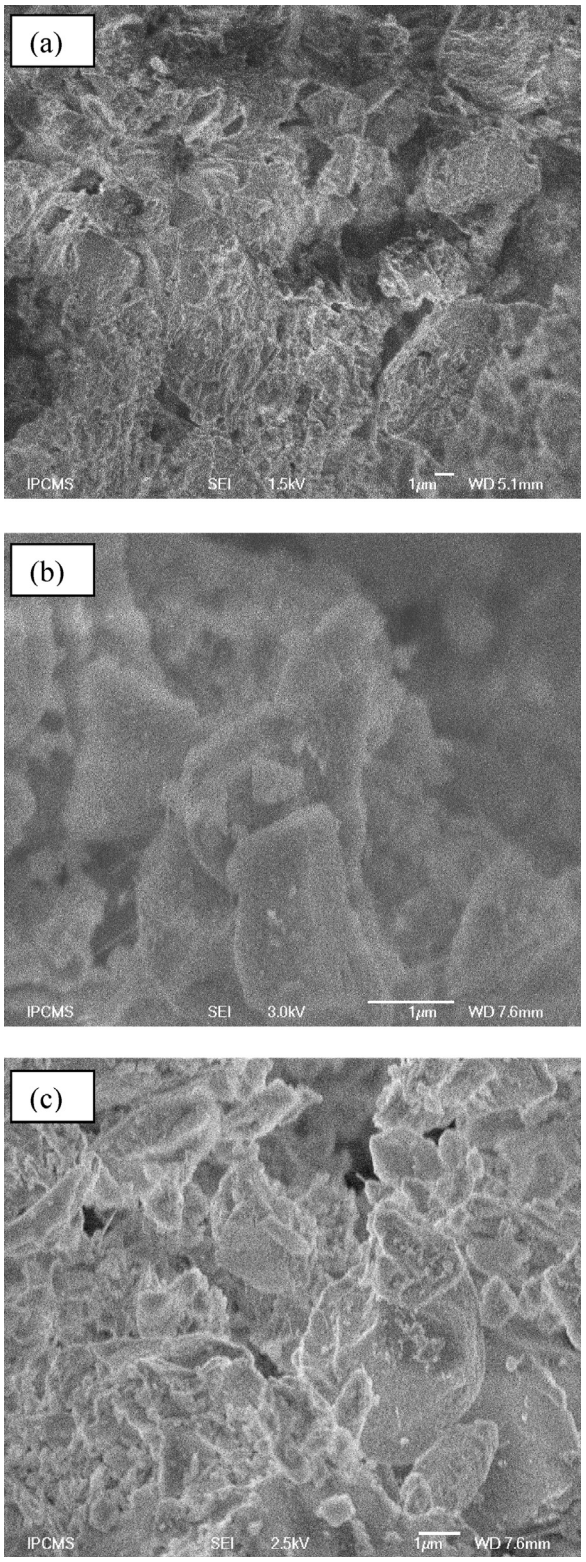

Fig. 4. SEM images of KIT-6 (a), 1 wt.%COOH/KIT-6 (b) and 10 wt.%COOH/KIT-6 (c).

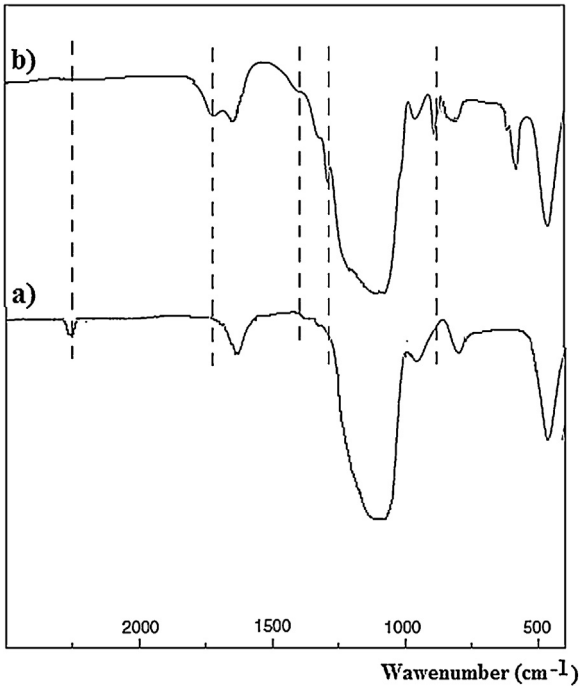

Fig. 5. IR spectrum of CN/KIT-6 (a) and 10 wt.%COOH/KIT-6 (b).

3.1.7. Dissociation constant of 10 wt.%COOH/KIT-6 materials

The dissociation constant, a means of analyzing the solid ion exchanger via the ion exchange reaction between a titrant counterion and a proton was calculated [68] for COOH/KIT-6. These protons are present in the ion exchanger and may dissociate the functional group in aqueous media before being neutralized in solution, as described by Eq. (3) with the equilibrium coefficient K_e (Eq. (4)):

$$\mathrm{RCOOH/KIT\text{-}6} + \mathrm{Na^+} + \mathrm{H_2O} \rightleftharpoons \mathrm{RCOO^-Na^+/KIT\text{-}6} + \mathrm{H_3O^+} \quad (3)$$

$$K_e = [\mathrm{RCOO^-Na^+/KIT\text{-}6}][\mathrm{H^+}]/[\mathrm{RCOOH/KIT\text{-}6}][\mathrm{Na^+}] \quad (4)$$

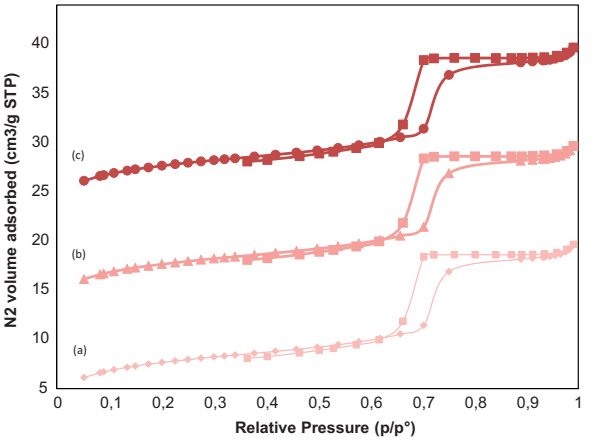

Fig. 6. (Color online). N_2 adsorption/desorption isotherms of 10 wt.%COOH/KIT-6–6 h (a), 24 h (b) and 240 h (c).

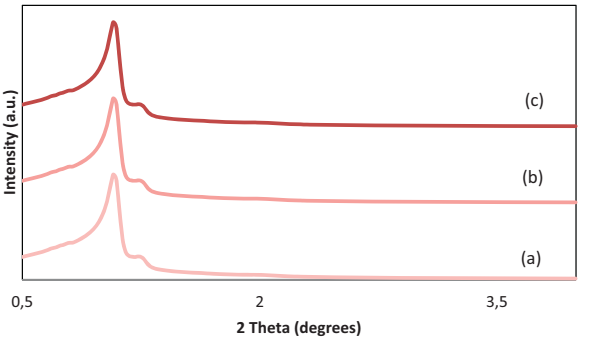

Fig. 7. (Color online). Low-angle XRD patterns of 10 wt.%COOH/KIT-6–6 h (a), 24 h (b) and 240 h (c).

The equilibrium coefficient, K_e, depended on the degree of neutralization for α, which equals the relative equivalent fraction of Na^+ in the ion exchanger at a given pH. At constant supporting electrolyte concentrations, the following Eq. (5) is valid:

$$-\log K = \mathrm{p}K_{\alpha=1/2} + (\mathrm{p}K_{\alpha-1} - \mathrm{p}K_{\alpha=0})(\alpha - 1/2) + m\log[\mathrm{Na^+}] \quad (5)$$

where m is a constant.

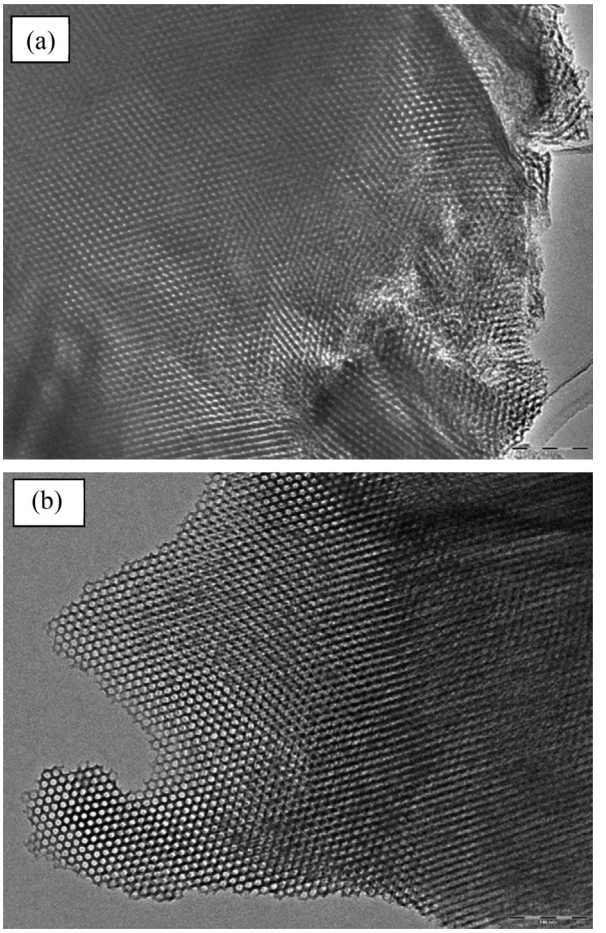

Fig. 8. TEM images of 10 wt.%COOH/KIT-6–6 h (a) and 240 h (c).

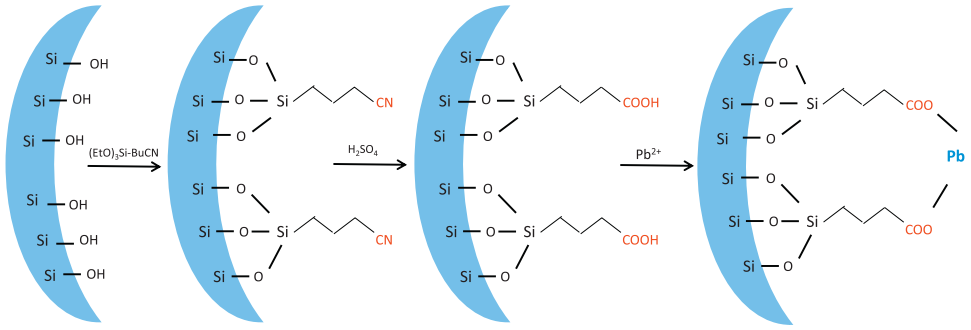

Scheme 2. Schematic illustration for the preparation of COOH/KIT-6 and the adsorption of Pb ions.

Accounting for a concentration of NaCl = 1 M, $-\log K$ was determined from the titration curve as the pH at half neutralization. The pK_a value of the COOH/KIT-6 sample was found to be 4.75. These results are consistent with other ones reported in the literature [58,69,70]. Based on the characterization results, we assumed that the COOH functional groups were grafted onto the KIT-6 surface. In such cases, the density of these groups is approximately 1.2 nm^{-2} and they are independent of each other. Because these functional groups are located on the nanopore surface, sorbents made using post-synthetic grafting techniques exhibit rapid adsorption kinetics.

3.2. Heavy-metal adsorption studies

The schematic representation for adsorption of metal ions is shown in Scheme 2.

3.2.1. Effect of contact time

The effect of time (from 0–300 min) on the Pb^{2+} sorption was determined by equilibrating the KIT-6 sorbate aliquot at pH 5.5 at 25, 30, and 35 °C (Fig. 9). The non-functionalized KIT-6 showed no ability to retain the Pb ions (Fig. 9), which suggests the importance of the functional groups. The efficiency of 10 wt.%COOH/KIT-6 for removing Pb^{2+} from the solution was determined from the Pb^{2+} adsorption rate, which may be associated with the wastewater cleanup efficiency. The adsorption rate curve

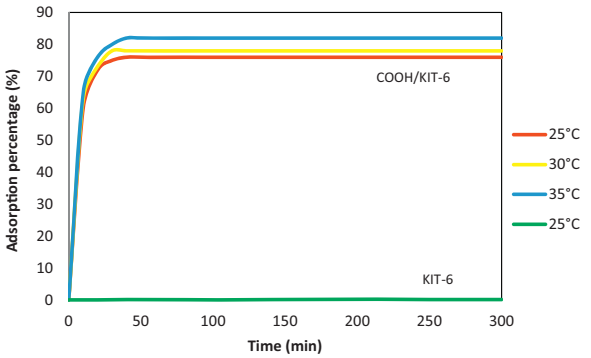

Fig. 9. (Color online). Influence of the contact time on the Pb(II) adsorption by KIT-6 and 10 wt.%COOH/KIT-6 at pH 5.5 and 25, 30 and 35 °C.

indicates that the Pb^{2+} adsorption was rapid (it occurred during the first 20 min of contact time) and nearly complete by 40 min with ca. 76–82% of the total Pb^{2+} having been adsorbed, at all studied temperatures. Increasing the contact time further yielded no further adsorption for 300 min. The COOH/KIT-6 sample clearly exhibited rapid kinetics for Pb^{2+} removal from an aqueous solution with a saturation time of 40 min. This COOH/KIT-6 adsorbent behavior may be explained by the presence of numerous vacant COOH/KIT-6 surface sites homogeneously distributed across the COOH/KIT-6 surface and within the inner porous structure. These sites were available for adsorption during the initial stages, which led to the rapid Pb^{2+} uptake increase. The sites have a high affinity for Pb^{2+} and can easily reach the adsorption sites where they are trapped, which rapidly fills these sites. Hence, the time required for rapid equilibrium is 40 min. However, a contact time of 100 min was used for every other study. As shown in Fig. 9, the adsorption capacity was almost identical across the three studied temperatures. Based on this study, a temperature of 25 °C was chosen for the following sections.

However, we cannot exclude the adsorption process after 300 min, which may be due, probably, to remaining vacant surface sites being difficult to occupy due to repulsion between the solute molecules in the solid and bulk phases. Probably, the breaking of such barrier forces (for further adsorption) is time dependent.

3.2.2. Effect of pH

The effect of pH on Pb(II) removal was investigated across a pH range from 2 to 7, at 25 °C as shown in Fig. 10. This figure indicates that Pb^{2+} uptake is pH dependent. Knowing the solution's pH was very important due to its influence on the adsorption process, taking into account that Pb species exist under the forms of Pb^{2+}, $Pb(OH)^{+}$, $Pb(OH)_2^{\circ}$, $Pb(OH)_3^{-}$ at different pH values [18,42,71,72]. A pH of 2.0 yields a poor adsorption performance (Fig. 10). COOH/KIT-6 adsorbed less Pb^{2+} (3.5%) onto its surface adsorption sites. The Pb^{2+} removal efficiency increased remarkably as the solution pH increased from 2 to 5.5, then increased slowly with further increases in pH. Increasing the solution pH weakened the complexation and more Pb was adsorbed by the COOH/KIT-6. In this case, the ions exchange interaction exists between the COOH/KIT-6 and Pb ions which favor adsorption. It must be noted that the

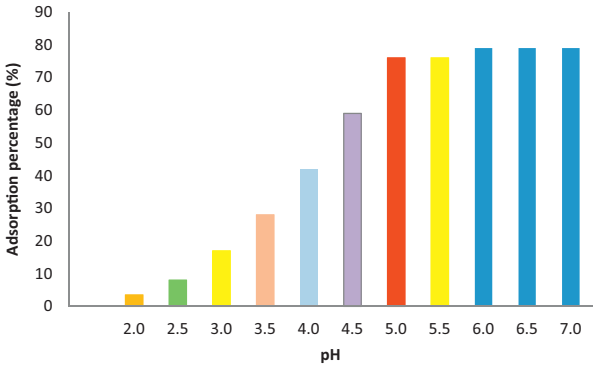

Fig. 10. (Color online). Effect of pH on Pb(II) adsorption.

calculated pKa of COOH/KIT-6 was 4.7. At pH values lower than the pKa values of 4.7, complexation occurs [73] and for pH values greater than the pKa, the functional groups are mainly in the dissociated form and exchange interaction exists between the COOH/KIT-6 and Pb. However, the possibility of Pb^{2+} ions precipitating during adsorption as hydroxides at the experimental pH was examined. We calculated the precipitation pH for Pb^{2+} as $Pb(OH)_2$ based on the product solubility (Eqs. (6) and (7)):

$$Pb(OH)_2 \rightarrow Pb^{2+} + 2\ OH^- \tag{6}$$

$$pH = 14 - \log[\sqrt{Pb^{2+}}/\sqrt{K_{sp}}] \tag{7}$$

We know the solubility product constant values (K_{sp}) for $Pb(OH)_2$ is 1.2×10^{-15} [74]; the calculated pH of precipitation for Pb^{2+} was approximately 7.1. These results indicate that the sorption of Pb^{2+} on COOH/KIT at pH > 7 is accomplished by concomitant precipitation of $Pb(OH)_2^0$ and sorption of $Pb(OH)^+$. At pH < 7, the Pb species is Pb^{2+} and the removal of Pb is accomplished by sorption.

To ensure a quantitative adsorption and avoid metal ion hydrolysis at higher pH values, a sample with a pH of 5.5 was chosen as the optimum one for these studies.

3.2.3. Model efficiency

The model efficiency [41], E, was calculated as follows:

$$E = 1 - \frac{\sum_{i=1}^{N} w_i \left(S_i - \hat{S}_i\right)^2}{\sum_{i=1}^{N} \left(S_i - \hat{S}_{wavg}\right)^2} \tag{8}$$

where $\hat{S}_{wavg}$ is the weighted mean of the measured values.

A model efficiency of 1 indicates a perfect fit to the data, whereas a model efficiency < 0 indicates averaging the measured values yields better predictions than the model.

This statistical measure is considered by many to be the best overall indicator of model fit because it has good resistance to errors due to extreme experimental values [41,75].

3.2.4. Error analysis

To evaluate and optimize the adsorption behavior [18,76], we used the coefficient of determination, r^2. The linear coefficient of determination was calculated from the sum of the square of $X(S_{xx})$, the sum of the square of $Y(S_{yy})$ and the sum of the square of $XY(S_{xy})$ as represented by the following equations (9) to (12):

$$r^2 = S_{xy}^2 / S_{xx} S_{yy} \tag{9}$$

$$S_{xx} = \sum_{i=1}^{n} x_i^2 - \left(\sum_{i=1}^{n} X_i\right)/n \tag{10}$$

$$S_{yy} = \sum_{i=1}^{n} y_i^2 - \left(\sum_{i=1}^{n} Y_i\right)/n \tag{11}$$

$$S_{xy} = \sum_{i=1}^{n} X_i y_i^2 - \left(\sum_{i=1}^{n} X_i\right)\left(\sum_{i=1}^{n} y_i\right)/n \tag{12}$$

These values may vary from 0 to 1. When the coefficient of determination is 1, 100% of the variation in adsorption capacity has been explained by the regression equation.

3.2.5. Adsorption kinetics

Adsorption kinetics is essential for wastewater treatment because it provides the necessary information on the reaction pathway and adsorption dynamics. The sorption behavior for Pb ions on 10 wt.%COOH/KIT-6 was verified using the Lagergren pseudo-first-order and chemisorption's pseudo-second-order kinetics models.

3.2.5.1. Pseudo-first-order model. Lagergren [77] showed that the adsorption rate of a solute on an adsorbent is based on the adsorption capacity. The pseudo-first-order rate expression is represented by the differential law:

$$dq_t/dt = k_1(q_e - q_t) \tag{13}$$

- k_1 is the pseudo-first-order rate constant;
- q_e is the adsorption capacity of the adsorbent ($mg \cdot g^{-1}$);
- q_t is the amount of Pb ion adsorbed at time t ($mg \cdot g^{-1}$).

By integrating for $t = 0$ to $t = t$ and $q_t = 0$ to $q_t = q_t$, we obtain the following linear expression:

$$\log(q_e - q_t) = \log q_e - \frac{k_1 t}{2} \cdot 303 \tag{14}$$

where k_1 is obtained from the slope of the plot of log $(q_e - q_t)$ versus t (Fig. 11).

3.2.5.2. Pseudo-second-order kinetics model. The pseudo-second-order reaction is greatly influenced by the amount of metal on the adsorbent's surface and adsorbed at equilibrium. This rate is directly proportional to the number of active surface sites. Huo [78] developed a pseudo-second-order kinetic expression for the sorption system of divalent metal ions, which we used to investigate the adsorption mechanism and rate constants for adsorbing Pb^{2+} to 10 wt.%COOH/KIT-6.

$$q_t = k q_e^2 t \tag{15}$$

$$dq_t/dt = k(q_e - q_t)^2/(1+kt) \tag{16}$$

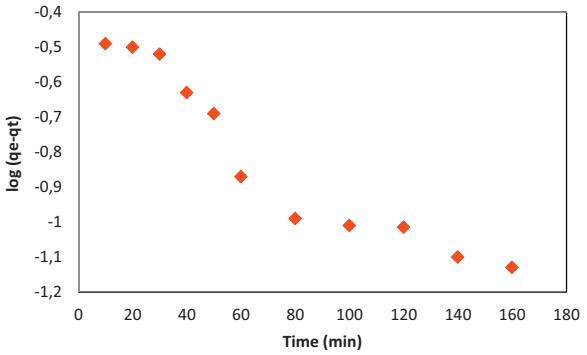

Fig. 11. Pseudo-first-order model fit for the adsorption of Pb(II) onto COOH/KIT-6.

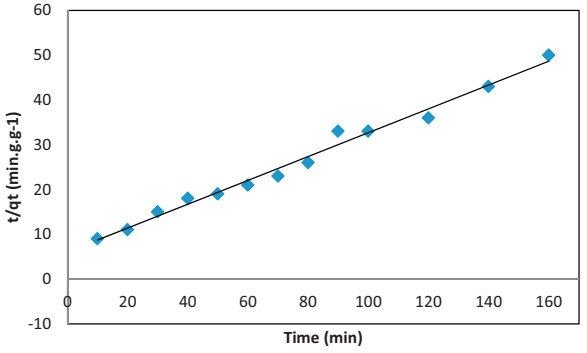

Fig. 12. Pseudo-second-order model fit for the adsorption of Pb(II) onto COOH/KIT-6.

$$^{1}/_{(q_e - q_t)} = kt + (^{1}/_{q_e}) \quad (17)$$

$$^{1}/_{q_t} = {}^{1}/_{q_e} + {}^{1}/_{kq_e^2} \quad (18)$$

where k is the rate constant of the pseudo-second-order equation (Fig. 12).

The pseudo-first-order and pseudo-second-order sorption kinetics parameters are shown in Table 2. The correlation coefficients for the pseudo-second-order model are much higher than those for the pseudo-first-order model. Therefore, the experimental values of q_e do not agree well with the calculated theoretical values. Thus, the sorption mechanism of the Pb(II) ion onto COOH/KIT-6 does not follow the pseudo-first-order kinetics model. The pseudo-first-order model is unsuitable for the sorption of Pb(II) onto COOH/KIT-6. The adsorbent system is described well by the pseudo-second-order kinetics model, which implies that the adsorption of Pb(II) onto COOH/KIT-6 may occur via a chemical process involving valence forces that share or exchange electrons.

3.2.6. Adsorption isotherms

The adsorption isotherm indicates how the adsorbed molecules are distributed between the liquid and solid phases when the adsorption process reaches equilibrium. Analyzing the isotherm data by fitting them to different models is important to determine which model is suitable for design purposes. In this study, the equilibrium experimental data for Pb(II) ions adsorbed onto the 10 wt.%COOH/KIT-6 beads were analyzed using the Langmuir and Freundlich models.

3.2.6.1. Langmuir isotherm model. The Langmuir model [79] assumes that a monomolecular layer forms when adsorption occurs without any interaction between the adsorbed molecules. All of the adsorption sites on the surface involved are assumed to be energetically identical, with no transmigration of the sorbate across the solid sorbent surface. In such cases, the intermolecular forces decrease as the distance from the adsorption surface increases.

The Langmuir equation may be written as follows:

$$q_e = \left(Q_{max} \;\; K_L C_e\right)/_{(1+K_L C_e)} \quad (19)$$

The expression for the linear form of Langmuir isotherm is as follows:

$$^{C_e}/_{q_e} = \left(^{1}/_{Q_{max}} \;\; K_L\right) + (^{C_e}/_{Q_{max}}) \quad (20)$$

where q_e is the equilibrium capacity of Pb(II) per unit weight of the adsorbent ($mg{\cdot}g^{-1}$), Q_{max} is the maximum adsorption capacity of the adsorbent corresponding to a complete monolayer coverage on the surface ($mg{\cdot}g^{-1}$), K_L is the Langmuir adsorption constant related to the energy of adsorption ($L{\cdot}mg^{-1}$), C_e is the equilibrium concentration of the solute in the bulk solution ($mg{\cdot}L^{-1}$).

Constants Q_{max} and K_L can be calculated from the intercepts and the slopes of the linear plots of C_e/q_e versus C_e. The above-mentioned parameters were obtained with the linear fitting procedure and are listed in Table 2.

3.2.6.2. Freundlich isotherm. The Freundlich model [80,81] is a commonly used model for analyzing adsorption data. Freundlich isotherm theory says that the ratio of solute adsorbed onto a given mass of sorbent to the solute concentration in solution is not constant across different

Table 2
Adsorption kinetics. Adsorption isotherms. Desorption efficiency.

Pseudo-first-order	Pseudo-second-order	Langmuir model	Freundlich model	Adsorption (%)	Desorption (%)
q_e, exp. = 3.8679 ($mg{\cdot}g^{-1}$)	q_e, exp. = 3.8679 ($mg.g^{-1}$)			75	95
q_e, calc. = 0.8742	q_e, calc. = 4.2559	q_{max} ($mg{\cdot}g^{-1}$) = 75.00	n = 2.8458	75	95
k_1 = 0.0158	k_2 = 0.0168	K_L ($L{\cdot}mg^{-1}$) = 0.0510	K_F = 4.7207	75	94
r^2 = 0.7727	r^2 = 0.9708	r^2 = 0.9903	r^2 = 0.9200	r^2 = 0.9976	r^2 = 0.9836
E^2 = 0.8002	E^2 = 0.9882	E^2 = 0.9976	E^2 = 0.9389	E^2 = 0.9987	E^2 = 0.9947

concentrations. This model is based on the relation between the adsorbed quantity and solute concentration at equilibrium, C_e. It describes non-ideal and reversible adsorption and is not restricted to a monolayer. This empirical model can be applied to multilayer adsorptions, with a non-uniform distribution for adsorption heat and affinity over a heterogeneous surface.

The Freundlich equation may be written as follows:

$$q_e = K_F C_e^{\frac{1}{n}} \quad (21)$$

A linear form of the Freundlich expression can be obtained by taking logarithms.

$$\log q_e = \log K_F + (1/n)\log C_e \quad (22)$$

where q_e is the amount of solute adsorbed per unit weight of adsorbent ($mg \cdot g^{-1}$), K_F is the Freundlich constant indicating the relative adsorption capacity for the adsorbent ($mg \cdot g^{-1}$), C_e is the equilibrium concentration of the solute in the bulk solution ($mg \cdot L^{-1}$) and $1/n$ is the heterogeneity factor indicating the adsorption intensity.

Several authors used the Langmuir and Freundlich isotherms for heavy metal sorption to several sorbents. Our results for the 10 wt.%COOH/KIT-6 are presented in Table 2. The Langmuir and Freundlich isotherm parameters and correlation coefficients are summarized. The coefficient of determination (R^2) was found to be 0.9903 for Pb(II) using the Langmuir model and 0.9200 for the Freundlich model. These results indicate that the metal ion adsorption to COOH/KIT-6 fitted the Langmuir model better than the Freundlich model, which may be due to the homogenous distribution of active sites on the COOH/KIT-6 surface because the Langmuir equation assumes a homogenous surface where all sites have equal adsorption energies. The $1/n$ values were between 0 and 1, which indicates that the Pb(II) adsorption to COOH/KIT-6 was favorable under the studied experimental conditions.

3.2.7. Desorption efficiency

Sorbent recovery is important to the mesoporous sorbent quality. The reversibility of Pb(II) adsorption to 10 wt.%COOH/KIT-6 was studied and the results and procedure are reported in Table 2. Pb(II) ions adsorbed to COOH/KIT-6 were effectively eluted using an HCl eluent. The highest recovery was found to be 95% using 1 M HCl. The results for the adsorption–desorption cycle demonstrated that COOH/KIT-6 could be reused up to 8 times without significantly changing the adsorption of the studied metal ions. Therefore, the prospects of COOH/KIT-6 are good for practical applications of removing Pb(II) from water and wastewater.

4. Conclusions

The ordered, functionalized mesoporous silica COOH/KIT, used to remove Pb^{2+} from polluted water, was prepared via a post-grafting pathway and characterized using several physicochemical techniques. The ability of COOH/KIT-6 to remove Pb(II) ions from aqueous solutions was analyzed via a batch technique. The optimum pH value for Pb(II) removal was 5.5. The adsorption of Pb to COOH/KIT-6 reached equilibrium within 40 min. The high r^2 values indicate that the Pb adsorption to COOH/KIT-6 follows a pseudo-second-order kinetics model based on the assumption that the rate-limiting step may be chemisorption. The Langmuir and Freundlich isotherm models for Pb(II) adsorption to COOH/KIT-6 were studied, and the Langmuir model best fits the adsorption data. –COOH groups covalently bonded to inorganic siliceous KIT-6 can be a new material for removing toxic metals from wastewater with high efficiency that can be economically regenerated while maintaining its high adsorption capacity.

Acknowledgements

The authors are indebted to T. Dintzer and O. Ersen for the kind assistance with the SEM and TEM images, respectively. We thank the Minister of Defense of Algeria and ICPEES Strasbourg, France, for their financial support.

References

[1] I. Fechete, Y. Wang, J.-C. Védrine, Catal. Today 189 (2012) 2.
[2] A. Torabi, T.H. Etsell, N. Semagina, P. Sarkar, Electrochim. Acta 67 (2012) 172.
[3] S.A. Skarlis, D. Berthout, A. Nicolle, C. Dujardin, P. Granger, Appl. Catal. B 148–149 (2014) 446.
[4] A. Djeddi, I. Fechete, F. Garin, Catal. Commun. 17 (2012) 173.
[5] P. Cozma, C. Ghinea, I. Mamaliga, W. Wukovits, A. Friedl, M. Gavrilescu, Clean Soil Air Water 41 (2013) 917.
[6] A. Djeddi, I. Fechete, F. Garin, Top. Catal. 55 (2012) 700.
[7] J. Shen, N. Semagina, ACS Catal. 4 (2014) 268.
[8] I.C. Marcu, M.N. Urlan, A. Rédey, I. Sandulescu, C. R. Chimie 13 (2010) 365.
[9] S.A. D'Ippolito, V.M. Benitez, V.M. Reyes, M.C. Rangel, C.L. Pieck, Catal. Today 172 (2011) 177.
[10] I. Fechete, P. Caullet, E. Dumitriu, V. Hulea, H. Kessler, Appl. Catal. A 280 (2005) 245.
[11] I. Popescu, A. Urda, T. Yuzhakova, I.C. Marcu, J. Kovacs, I. Sandulescu, C. R. Chimie 12 (2009) 1072.
[12] E. Dumitriu, V. Hulea, I. Fechete, C. Catrinescu, A. Auroux, J.-F. Lacaze, C. Guimon, Appl. Catal. A 181 (1999) 15.
[13] S. Nassreddine, S. Casu, J.L. Zotin, C. Geantet, L. Piccolo, Catal. Sci. Technol. 1 (2011) 408.
[14] D. Meloni, R. Monaci, E. Rombi, C. Guimon, H. Martinez, I. Fechete, E. Dumitriu, Stud. Surf. Sci. Catal. 142A (2002) 167.
[15] S. Vasudevan, F. Epron, J. Lakshmi, S. Ravichandran, S. Mohan, G. Sozhan, Clean Soil Air Water 38 (2010) 225.
[16] I. Georgescu, M. Mureseanu, G. Carja, V. Hulea, J. Environ. Eng. 139 (2013) 1285.
[17] C. Hristodor, V. Copcia, D. Lutic, E. Popovici, Rev. Chim. 61 (2010) 285.
[18] A.E. Ofomaja, E.I. Unuabonah, N.A. Oladoja, Biores. Technol. 101 (2010) 3844.
[19] R.M. Hlihor, M. Diaconu, D. Fertu, C. Chelaru, I. Sandu, T. Tavares, M. Gavrilescu, Int. J. Environ. Res. 7 (2013) 581.
[20] L. Bulgariu, A. Ceica, L. Lazar, I. Cretescu, I. Balasanian, Rev. Chim. 61 (2010) 1136.
[21] B. Koubaissy, J. Toufaily, M. El-Murr, T. Hamieh, P. Magnoux, G. Joly, Phys. Procedia 21 (2011) 220.
[22] A. Shahbazi, H. Younesi, A. Badiei, Chem. Eng. J. 168 (2011) 505.
[23] E. Da'na, A. Sayari, Desalination 285 (2012) 62.
[24] S. Moulay, N. Bensacia, F. Garin, I. Fechete, A. Boos, Adsorpt. Sci. Technol. 81 (2013) 691.
[25] M. Amini, H. Younesi, N. Bahramifar, Colloids Surf. Physicochem. Eng. Aspects 337 (2009) 67.
[26] Ö. Gercel, H.F. Gercel, Chem. Eng. J. 132 (2007) 289.
[27] O.K. Júnior, L.V.A. Gurgel, R.P. de Freitas, L.F. Gil, Carbohydr. Polym. 77 (2009) 643.
[28] M. Mureseanu, A. Reiss, I. Stefanescu, E. David, V. Parvulescu, G. Renard, V. Hulea, Chemosphere 73 (2008) 1499.
[29] B. Volesky, Biosorption of Heavy Metals, CRC Press, Boca Raton, FL, USA, 1990.
[30] R. Naseem, S.S. Tahir, Water Res. 35 (2001) 3982.

[31] R.W. Rousseau, Handbook of Separation Process Technology, Wiley, New York, 1987.
[32] D. Pérez-Quintanilla, A. Sánchez, I. del Hierro, M. Fajardo, I. Sierra, J. Colloid Interface Sci. 313 (2007) 551.
[33] M. Amini, H. Younesi, N. Bahramifar, Colloids Surf., A 337 (2009) 67.
[34] A. Khelifa, S. Aoudj, S. Moulay, M. De Petris-Wery, Chem. Eng. Proc. Proc. Intensif. 70 (2013) 110.
[35] T.S. Anirudhan, L. Divya, M. Ramachandran, J. Hazard. Mater. 157 (2008) 620.
[36] M.C. Basso, E.G. Cerrella, A.L. Cukierman, Ind. Eng. Chem. Res. 41 (2002) 3580.
[37] H. Parab, S. Joshi, N. Shenoy, R. Verma, A. Lali, M. Sudersanan, Biores. Technol. 96 (2005) 1241.
[38] V. Hernandez-Morales, R. Nava, Y.J. Acosta-Silva, S.A. Macias-Sanchez, J.J. Perez-Bueno, B. Pawelec, Micropor. Mesopor. Mater. 160 (2012) 133.
[39] M. Sciban, M. Klasmja, B. Skrbic, J. Hazard. Mater. 136 (2006) 266.
[40] E.I. Unuabonah, B.I. Olu-Owolabi, K.O. Adebowale, A.E. Ofomaja, Colloids Surf., A Physicochem. Eng. Aspects 292 (2007) 202.
[41] B.I. Olu-Owolabi, E.I. Unuabonah, J. Hazard. Mater. 184 (2010) 731.
[42] R. Wang, Q. Li, D. Xie, H. Xiao, H. Lu, Appl. Surf. Sci. 279 (2013) 129.
[43] X.-L. Wang, A. Mei, M. Li, Y. Lin, C.-W. Nan, Solid State Ionics 177 (2006) 1287.
[44] T. Tsoncheva, J. Rosenholm, M. Linden, F. Kleitz, M. Tiemann, L. Ivanova, M. Dimitrov, D. Paneva, I. Mitov, C. Minchev, Microporous Mesoporous Mater. 112 (2008) 327.
[45] I. Fechete, B. Donnio, O. Ersen, T. Dintzer, A. Djeddi, F. Garin, Appl. Surf. Sci. 257 (2011) 2791.
[46] J. Perez-Pariente, I. Diaz, F. Mohio, E. Sastre, Appl. Catal. A-Gen. 254 (2003) 173.
[47] D.A. Ponomoreva, V.V. Yuschenko, I.I. Ivanova, L. Pasqua, F. Testa, F. Di Renzo, F. Fajula, Stud. Surf. Sci. Catal. 154C (2004) 2208.
[48] I. Fechete, O. Ersen, F. Garin, L. Lazar, A. Rach, Catal. Sci. Technol. 3 (2013) 444.
[49] J. Wang, S.Y. Chew, Z.W. Zhao, S. Ashraf, D. Wexler, J. Chen, S.H. Ng, S.L. Chou, H.K. Liu, Carbon 46 (2008) 229.
[50] C. Yuan, B. Gao, L. Su, X. Zhang, J. Colloid Interface Sci. 322 (2008) 545.
[51] M. Mureseanu, A. Reiss, N. Cioatera, I. Trandafir, V. Hulea, J. Hazard. Mater. 182 (2010) 197.
[52] C. Delacôte, F.O.M. Gaslian, B. Lebeau, A. Walcarius, Talanta 79 (2009) 877.
[53] S.A. Idris, S.R. Harvey, L.T. Gibson, J. Hazard. Mater. 193 (2011) 171.
[54] I. Sierra, D. Perez-Quintanilla, Chem. Soc. Rev. 42 (2013) 3792.
[55] H. Wan, L. Liu, C. Li, X. Xue, X. Ling, J. Colloid Interface Sci. 337 (2009) 420.
[56] P. Shah, N. Sridevi, A. Prabhune, V. Ramaswamy, Microporous Mesoporous Mater. 116 (2008) 157.
[57] A. Katiyar, S. Yadav, P.G. Smirniotis, N.G. Pinto, J. Chromatogr. A 1122 (2006) 13.
[58] M.C. Bruzzoniti, A. Prelle, C. Sarzanini, B. Onida, S. Fiorilli, E. Garrone, J. Sep. Sci. 30 (2007) 2414.
[59] J.M. Rosenholm, T. Czuryszkiewicz, F. Kleitz, J.B. Rosenholm, M. Linden, Langmuir 23 (2007) 4315.
[60] W. Xu, Q. Gao, Y. Xu, D. Wu, Y. Sun, W. Shen, F. Deng, J. Solid State Chem. 181 (2008) 2837.
[61] C. Yang, Y. Wang, B. Zibrowius, F. Schuth, Phys. Chem. Chem. Phys. 6 (2004) 2461.
[62] X.G. Wang, K.S.K. Lin, J.C.C. Chan, S. Cheng, J. Phys. Chem. B 109 (2005) 1763.
[63] F. Kleitz, S.H. Choi, R. Ryoo, Chem. Commun. (2003) 2136.
[64] A. Boulaoued, I. Fechete, B. Donnio, M. Bernard, P. Turek, F. Garin, Microporous Mesoporous Mater. 155 (2012) 131.
[65] X.S. Zhao, G.Q. Lu, A.J. Whittaker, G.J. Miller, H.Y. Zhu, J. Phys. Chem. B 101 (1997) 6525.
[66] A. Prabhu, L. Kumaresan, M. Palanichamy, V. Murugesan, Appl. Catal. A 360 (2009) 59.
[67] S.J. Gregg, K.S.W. Sing, Adsorption, Surface Area and Porosity, second ed., Academic Press, London, 1982.
[68] V.S. Soldatov, React. Funct. Polym. 46 (2000) 55.
[69] S. Fiorilli, B. Onida, B. Bonelli, E. Garrone, J. Phys. Chem. B 109 (2005) 16725.
[70] R.C. West, Handbook of Chemistry and Physics, 55th ed., 1974–1975, CRC Press, Cleveland, Ohio, USA, 1974.
[71] D. Xu, X. Tan, C. Chen, X. Wang, J. Hazard. Mater. 154 (2008) 407.
[72] J. Huang, M. Ye, Y. Qu, L. Chu, R. Chen, Q. He, D. Xu, J. Colloid Interface Sci. 385 (2012) 137.
[73] E. Fourest, B. Volesky, Environ. Sci. Technol. 30 (1996) 277.
[74] J.A. Dean, Lange's Handbook of Chemistry, 15th ed., McGraw-Hill, 1999.
[75] C.H. Bolster, G.M. Hornberger, Soil Sci. Soc. Am. J. 71 (2006) 1796.
[76] B. Boulinguiez, P. Le Cloirec, D. Wolbert, Langmuir 24 (2008) 6420.
[77] S. Lagergren Zur, K. Sven. Vetenskapsakad. Handl. 24 (1898) 1.
[78] Y.S. Ho, G. McKay, Process Biochem. 34 (1999) 451.
[79] I. Langmuir, J. Am. Chem. Soc. 38 (1916) 2221.
[80] H.M.F. Freundlich, J. Phys. Chem. 57 (1906) 385.
[81] A.W. Adamson, A.P. Gast, Physical Chemistry of Surfaces, sixth ed., Wiley-Interscience, New York, 1997.